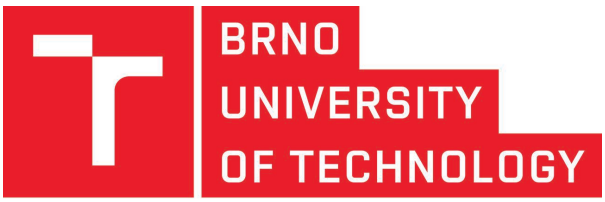

BRNO UNIVERSITY OF TECHNOLOGY
VYSOKÉ UČENÍ TECHNICKÉ V BRNĚ

CENTRAL EUROPEAN INSTITUTE OF TECHNOLOGY
STŘEDOEVROPSKÝ TECHNOLOGICKÝ INSTITUT

SPECIAL PROBLEMS OF FRACTURE MECHANICS OF SINGULAR STRESS CONCENTRATORS IN COMPOSITE MATERIALS

SPECIÁLNÍ PROBLÉMY LOMOVÉ MECHANIKY SINGULÁRNÍCH KONCENTRÁTORŮ NAPĚTÍ V KOMPOZITNÍCH MATERIÁLECH

DOCTORAL THESIS SUMMARY
TEZE DISERTAČNÍ PRÁCE

AUTHOR
AUTOR PRÁCE
Ing. ONDŘEJ KREPL

SUPERVISOR
VEDOUCÍ PRÁCE
doc. Ing. JAN KLUSÁK, Ph.D.

BRNO 2018

Preface

The dissertation "Special problems of fracture mechanics of singular stress concentrators in composite materials" is the culmination of my doctoral studies and research in the fracture mechanics. Its creation started during my research internship in Paris in the autumn of 2016 and ended in the beggining of 2018, although much of the theoretical work was developed earlier at the time of my doctoral study, which initiated in 2013.

It would have been very difficult or even impossible without the support and advice of some great people. First of all, I would like to thank my supervisor doc. Ing. Jan Klusák, Ph.D. for his excellent guidance the whole time of my PhD study. I am very grateful to him for everything he has taught me, the inspiration he provided and I truly appreciate his support. I would also like to thank Prof. Dominique Leguillon for his professional guidance during the research internship in France. Last but not least, I would like to thank doc. Ing. Tomáš Profant, Ph.D. who introduced me about eight years ago in the fascinating field of the fracture mechanics.

The author would like to thank the Czech Science Foundation for financial support through the Grant 16/18702S. The research within the dissertation has been financially supported by the Ministry of Education, Youth and Sports of the Czech Republic under the project CEITEC 2020 [LQ1601].

Keywords

Fracture mechanics, general singular stress concentrator, bi-material notch, sharp material inclusion, composite material

Klíčová slova

Lomová mechanika, obecný singulární koncentrátor napětí, bi-materiálový vrub, ostrá materiálová inkluze, kompozitní materiál

CEITEC IPM, Institute of Physics of Materials AS CR

Žižkova 22, Brno 616 62, Czech Republic

krepl@ipm.cz

Contents

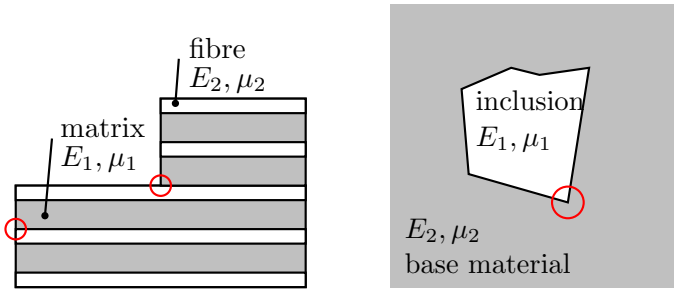

Figure 1: Left-hand side: Locations in a composite material where a singular stress concentration is expected. Right-hand side: Sharp material inclusion tip where a singular stress concentration is expected

1. Introduction

Fracture mechanics has been developed following the fact that the majority of components and structures in engineering application contain cracks or crack-like flaws [1]. Linear elastic fracture mechanics (LEFM) uses methods of the linear elastic stress analysis of a cracked part to determine the conditions under which a crack, or crack-like flaw will extend. The linear elastic analysis of a body with a crack shows that the stresses around the crack tip vary according to $r^{-1/2}$ where r is the distance from the crack tip. It is obvious that the elastic stresses become unbounded as r approaches the crack tip [2, 3].

As a result of the near tip stress field character of a crack, it is among so called singular stress concentrators. A crack can be conceived as a special case of a sharp V-notch with an opening angle equal to zero. It has been found that the stress field in the vicinity of a sharp V-notch tip (with a non-zero opening angle) also has the singular character, nonetheless different from the case of a crack [8]. The singular stress concentrators discussed above originate from a discontinuity in geometry. However, singular stress character in a body different from a crack can also arise from a material properties discontinuity. This may be the case of a bi-material junction which is a model for a sharp polygon-like inclusion embodied in a parent material, Figure 1. An ultimate case of a singular stress concentrator a sharp bi-material notch is the case combining both geometrical and material discontinuities.

Nowadays we encounter a rising number of components and structures made out of composite materials. The composite materials (or composites) consist of two or more combined constituents that are combined at a macroscopic level [6]. One constituent is called the *reinforcing phase* and the one in which the reinforcement is embedded is called the *matrix* as shown in Figure 1. The reinforcing phase material may be in the form of fibers, particles, or flakes. One of the reasons to choose composites is that for example monolithic metals and their alloys cannot always meet the demands of today's advanced technologies. Only by combining several materials can the performance requirements be met as we can see in the aerospace industry where a combination of supreme structural characteristics and low weight is critical. On the other hand, the very nature of composites (the material properties mismatch) brings higher complexity of their description in terms of fracture mechanics.

Advanced studies of the linear elastic fracture mechanics of cracks show an influence of particular singular and non-singular stress series terms on the fracture behavior of solids with a crack. It is shown in literature that the first non-singular (constant) term of Williams' stress series [9] called T-stress plays an important role within crack behavior assessment both in the case of brittle fracture and in the case of fatigue crack propagation [11, 12, 13, 14]. Similarly, the effects of the T-stress on interfacial cracks in isotropic bi-materials were studied [15].

Contrary to this, the approaches that will be able to assess the influence of the non-singular stress terms on a fracture initiation in the general singular stress concentrators are in the focal point to be developed. The following stress concentrators are considered: the sharp V-notch, the sharp bi-material notch and the bi-material junction. In the case of the general stress concentrators, the influence of the non-singular terms has not been studied sufficiently, but it is expected as well. The stress concentrators mentioned above can model a number of typical dangerous points of components usually responsible for their failure.

Depending on loading conditions and geometry of a component with the stress concentrator, a generalized constraint can have a positive or negative influence. It can counteract crack initiation or it can stimulate it. Thus assessment not covering the influence of the constraint provides overestimated or underestimated results. In the first case the new approaches can save a certain volume of material, while in the second case the new stability assessment can prevent a fatal damage. Thus the results of the future research can raise the credibility and extend the application possibilities of the fracture mechanics.

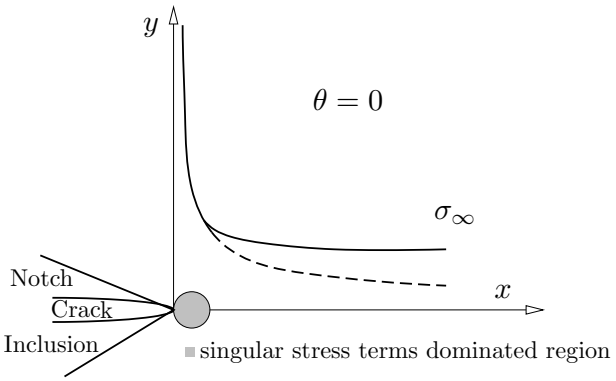

Figure 2: Region of domination of singular terms ahead of a crack and a notch or an inclusion, where stress is precisely described by singular terms only. Dashed line describes the singular terms solution.

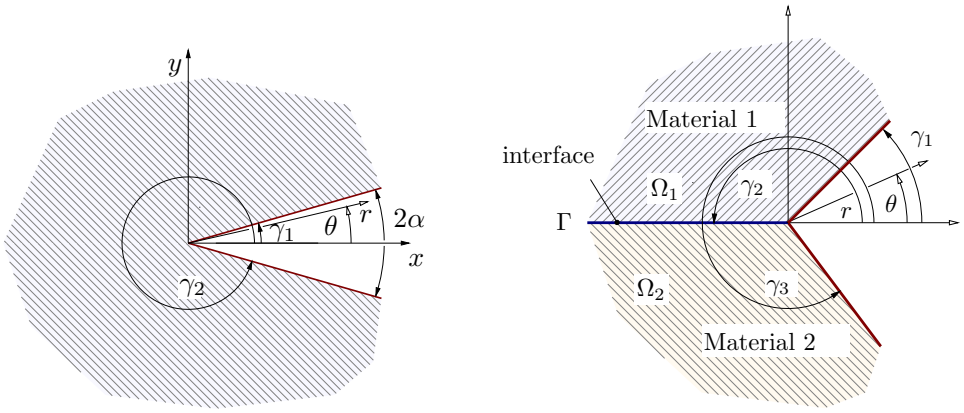

Figure 3: V-notch in the left-hand side, bi-material notch in the right-hand side.

2. Methods and results

2.1. Limitations of single-parameter fracture mechanics

The area near the crack in which the stress field is precisely described only by a singular term is known as the K-dominated region (in the case of fracture mechanics of cracks). A similar region can be found near the notch tip or the sharp material inclusion tip, and it is again a region where the singular stress terms dominate as illustrated in Figure 2. This region with dominating singular terms is one of the building blocks of classic fracture mechanics. Some of crack initiation criteria of generalized stress concentrators require establishing a specific distance from the tip of the concentrator, which depends on material characteristics (the strength and fracture toughness of the material [23] or the size of material grain, [18, 19]). In fact, these distances are in some cases much larger than the characteristic dimension of the domain of prevailing singular stress terms [16, 17, 21, 22]. This means that a description only by a singular term may not be sufficient to describe stresses precisely enough and therefore to assess reliably the stability of a dangerous point. Single-parameter fracture mechanics is not sufficient in the case of assessment of crack initiation and propagation in silicate-based composites. In these quasi-brittle materials a fracture process zone ahead of a crack has a larger size (in the order of millimeters) than a plastic zone occurring in the case of metallic materials (typically from micrometers to 1 mm). For this reason, stress distribution must be described reliably in a larger area ahead of the stress concentrator by singular and non-singular terms.

2.2. Fracture mechanics of V-notch and bi-material notch

A V-notch and bi-material notch are shown in Figure 3. The geometry of a V-notch is characterized by the angles γ_1 and γ_2 and complementary opening angle 2α. The case of a bi-material notch has three geometric parameters γ_1, γ_2 and γ_3 and complementary opening angle 2α. The material properties are given by the elastic constants of

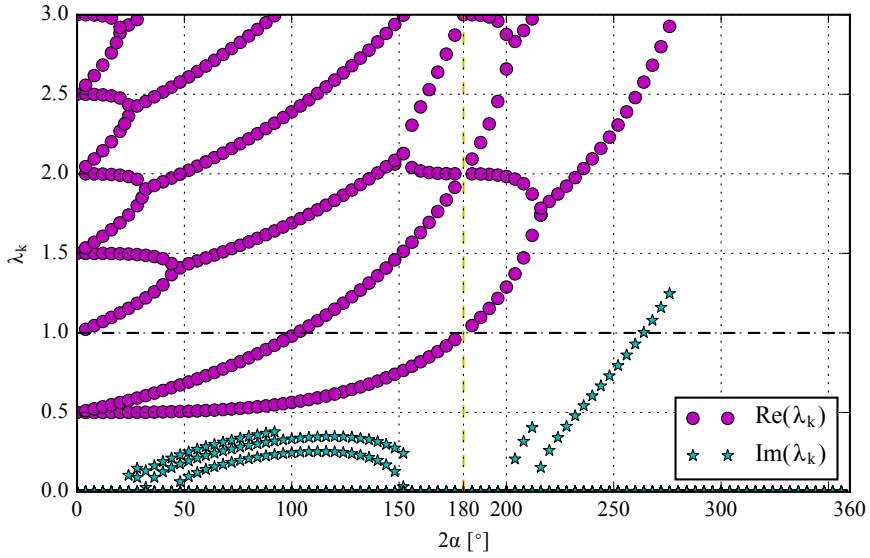

Figure 4: Dependence of eigenvalues λ_k of the V-notch on the opening angle 2α. The black dashed line divides the graph into fields where singular and non-singular eigenvalues are found. The yellow dashed line represents notch free plate.

Young's moduli and Poisson's ratios. The solution mostly presupposes the approximation of plane strain or plane stress. For the case of a bi-material notch a perfect bonding (displacement and traction continuity) is assumed at the interface. Furthermore, the notch surfaces are traction-free. Stress distribution in the case of a V-notch or bi-material notch [17, 27] is given by:

$$\sigma_{ij}\left(r,\theta\right) \quad = \quad \sum_{k=1}^{\infty}\left\{H_k r^{\lambda_k-1} f_{ijk}(\theta) + \bar{H}_k r^{\bar{\lambda}_k-1} \bar{f}_{ijk}(\theta)\right\}. \tag{1}$$

where the indices $(i,j) \equiv (r,\theta)$ are polar coordinates. The symbol H_k stands for the Generalized Stress Intensity Factor (GSIF) with the unit of $[H_k] = \mathrm{MPa}\,.\,\mathrm{m}^{1-\lambda_k}$. The $f_{ijk}\left(\theta\right)$ is the angular eigenfunction, which is dimensionless. The stress terms exponents $1-\lambda_k$, where λ_k is the kth eigenvalue of the problem are in general complex. In most of the geometrical and material configurations of V-notches and bi-material notches there are two real singular stress terms exponents in the interval $(0,1)$ corresponding to the singular terms of the series [28]. Eigenvalues with the real part greater than 1 correspond to the higher order terms (non-singular). The stress terms exponents are dependent only on the local geometry of the problem. The boundary conditions of the V-notch correspond to the zero traction on the notch free surfaces. Similarly, the boundary conditions for the bi-material notch are based on zero traction on the notch free surfaces as well as the displacement and traction continuity through the interface. The determination of eigenvalues λ_k is virtually identical for the case of a V-notch or a bi-material notch. It is based on the solution of the eigenvalue problem:

$$\mathbf{A}\left(\lambda\right) v \quad = \quad \mathbf{0}, \tag{2}$$

The general dependence of eigenvalues λ_k on the opening angle 2α is shown in Figure 4 for a V-notch and in Figure 5 for a bi-material notch. Note, that in the case of the V-notch for angle $2\alpha \sim 103°$ the eigenvalue $\lambda_2 = 1$. For larger angles 2α, the term associated with eigenvalue λ_2 is always a non-singular one. This is in accordance with results of Ayatollahi and Nejati in [36] who report the angle value of 102.55°. The generalized stress intensity factors H_k are dependent on the global geometry and the loading. Methods of its calculation are the combination of numerical and analytical approaches. One of the possible method of its determination is the path independent Ψ-integral by which the kth GSIF can be calculated as:

$$H_k \quad = \quad \frac{\Psi(u^{\mathrm{FE}}(\theta), r^{-\lambda_k} f_{ik}^{-}(\theta))}{\Psi(r^{\lambda_k} f_{ik}(\theta), r^{-\lambda_k} f_{ik}^{-}(\theta))}. \tag{3}$$

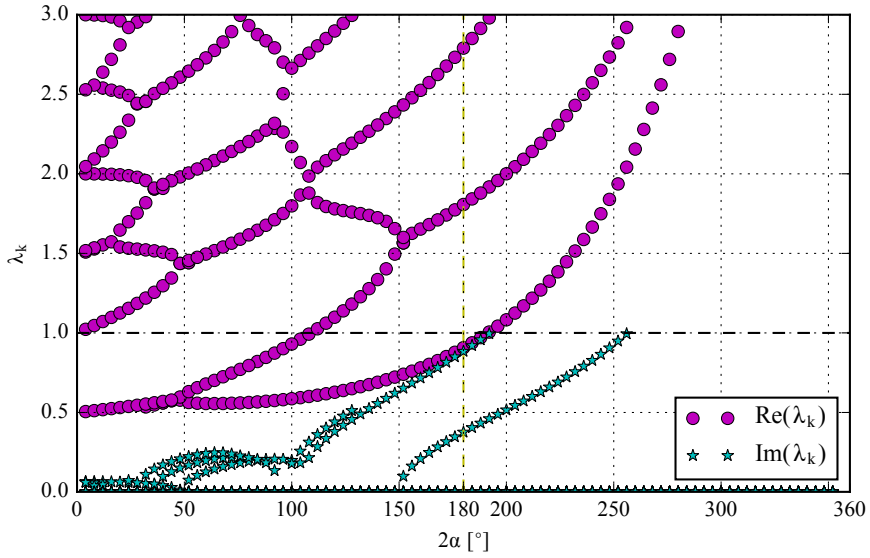

Figure 5: Dependence of eigenvalues λ_k of the bi-material notch on the opening angle 2α. The black dashed line divides the graph into fields where singular and non-singular eigenvalues are found. The yellow dashed line represents the free edge singularity. The geometry of studied case is $\gamma_1 = \alpha$, $\gamma_2 = \pi$, $\gamma_3 = 2\pi - \alpha$. The Young's moduli ratio is $E_1/E_2 = 0.25$ and Poisson's ratio is $\nu_1 = \nu_2 = 0.25$.

Because of the Ψ-integral path independence the analytical term in denominator $\Psi_k^{\text{analyt}} = \Psi(r^{\lambda_k} f_{ik}(\theta), r^{-\lambda_k} f_{ik}^{-}(\theta))$ can be calculated once for all for given problem. The term in the numerator $\Psi_k^{\text{FE}} = \Psi(u^{\text{FE}}(\theta), r^{-\lambda_k} f_{ik}^{-}(\theta))$ is calculated from the finite element results. Another method of GSIFs determination is the overdeterministic method. The ODM belongs to so called direct methods and is based on the least-squares solution of overdetermined system of linear equations. In the general case of $H_k \in \mathbb{C}$ the system has the following form:

$$
\begin{bmatrix}
\Re\{f_{rr1}(\theta_1) r^{\lambda_1}\} & \Im\{f_{rr1}(\theta_1) r^{\lambda_1}\} & \dots & \Re\{f_{rrn}(\theta_1) r^{\lambda_n}\} & \Im\{f_{rrn}(\theta_1) r^{\lambda_n}\} \\
\Re\{f_{rr1}(\theta_2) r^{\lambda_1}\} & \Im\{f_{rr1}(\theta_2) r^{\lambda_1}\} & \dots & \Re\{f_{rrn}(\theta_2) r^{\lambda_n}\} & \Im\{f_{rrn}(\theta_2) r^{\lambda_n}\} \\
\vdots & \vdots & & \vdots & \vdots \\
\Re\{f_{rr1}(\theta_m) r^{\lambda_1}\} & \Im\{f_{rr1}(\theta_m) r^{\lambda_1}\} & \dots & \Re\{f_{rrn}(\theta_m) r^{\lambda_n}\} & \Im\{f_{rrn}(\theta_m) r^{\lambda_n}\} \\
\Re\{f_{r\theta1}(\theta_1) r^{\lambda_1}\} & \Im\{f_{r\theta1}(\theta_1) r^{\lambda_1}\} & \dots & \Re\{f_{r\theta n}(\theta_1) r^{\lambda_n}\} & \Im\{f_{r\theta n}(\theta_1) r^{\lambda_n}\} \\
\Re\{f_{r\theta1}(\theta_2) r^{\lambda_1}\} & \Im\{f_{r\theta1}(\theta_2) r^{\lambda_1}\} & \dots & \Re\{f_{r\theta n}(\theta_2) r^{\lambda_n}\} & \Im\{f_{r\theta n}(\theta_2) r^{\lambda_n}\} \\
\vdots & \vdots & & \vdots & \vdots \\
\Re\{f_{r\theta1}(\theta_m) r^{\lambda_1}\} & \Im\{f_{r\theta1}(\theta_m) r^{\lambda_1}\} & \dots & \Re\{f_{r\theta n}(\theta_m) r^{\lambda_n}\} & \Im\{f_{r\theta n}(\theta_m) r^{\lambda_n}\} \\
\Re\{f_{\theta\theta1}(\theta_1) r^{\lambda_1}\} & \Im\{f_{\theta\theta1}(\theta_1) r^{\lambda_1}\} & \dots & \Re\{f_{\theta\theta n}(\theta_1) r^{\lambda_n}\} & \Im\{f_{\theta\theta n}(\theta_1) r^{\lambda_n}\} \\
\Re\{f_{\theta\theta1}(\theta_2) r^{\lambda_1}\} & \Im\{f_{\theta\theta1}(\theta_2) r^{\lambda_1}\} & \dots & \Re\{f_{\theta\theta n}(\theta_2) r^{\lambda_n}\} & \Im\{f_{\theta\theta n}(\theta_2) r^{\lambda_n}\} \\
\vdots & \vdots & & \vdots & \vdots \\
\Re\{f_{\theta\theta1}(\theta_m) r^{\lambda_1}\} & \Im\{f_{\theta\theta1}(\theta_m) r^{\lambda_1}\} & \dots & \Re\{f_{\theta\theta n}(\theta_m) r^{\lambda_n}\} & \Im\{f_{\theta\theta n}(\theta_m) r^{\lambda_n}\}
\end{bmatrix}
\begin{bmatrix}
\Re\{H_1\} \\ \Im\{H_1\} \\ \Re\{H_2\} \\ \Im\{H_2\} \\ \vdots \\ \Re\{H_n\} \\ \Im\{H_n\}
\end{bmatrix}
= \mathbf{S}_{[3m]}^{\text{FE}}.
$$

The matrix on the left-hand side is formed of the known analytical eigenfunctions. On the left-hand side we also find the unknown vector of n GSIFs. The right-hand side vector consists of radial, shear and tangential stress components, determined by FE. For an overdetermined system of stress based linear equations above that is in a short form written:

$$\mathbf{F}_{[3m\times n]}\mathbf{H}_{[n]} = \mathbf{S}_{[3m]}^{\text{FE}}, \tag{4}$$

no exact solution exists since $3m > n$. The approximation of the solution is found by minimizing the residual vector by least squares method. The method can be also based on displacements, which is in short form written:

$$\mathbf{F}_{[2m\times n]}\mathbf{H}_{[n]} = \mathbf{u}_{[2m]}^{\text{FE}}. \tag{5}$$

The displacement based method is in some cases preferred due to higher inherent precision of displacement based FE codes. The theoretical and numerical derivation of both λ_k and H_k is in detail commented in the dissertation.

Criteria of crack initiation direction and stability criteria

A V-notch, bi-material notch and a crack in homogeneous material are all the singular stress concentrators. Thus we suppose that the mechanism of crack initiation in a V-notch or bi-material notch is the same as the mechanism of crack propagation in single material. The criteria of the direction of crack initiation at a V-notch or bi-material notch tip and the criteria of the stability of a V-notch or bi-material notch are derived in analogy to the approaches of a crack in homogeneous material. The classic fracture mechanics approach of comparison of the stress intensity factor K_{I} with its critical value K_{Icrit} is generalized to the following relation:

$$H_1\left(\sigma_{\mathrm{appl}}\right) \quad < \quad H_{1,\mathrm{crit}}\left(K_{\mathrm{Icrit}}\right). \tag{6}$$

A crack is not initiated at the notch tip if the value H_1 is lower than its critical value $H_{1,\mathrm{crit}}$. The value $H_1\left(\sigma_{\mathrm{appl}}\right)$ follows from a numerical solution and depends mainly on the level of external loading and on the global geometry. Its critical value $H_{1,\mathrm{crit}}$ depends on the critical material characteristic K_{IC} or K_{Ith} and has to be deduced with the help of the controlling variable L, see [41]. The controlling variable L needs to have a clear and identical physical meaning in the case of assessing both a crack in homogeneous material and a V-notch or bi-material notch. With respect to particularities of a V-notch or bi-material notch following controlling variables L were chosen: (i) the mean value of the stress component $\sigma_{\theta\theta}$ and (ii) the mean value of the strain energy density factor Σ. In this work we use multi-parameter approach, which consider first n terms of the stress series. Contrary to the case of a crack, direction of maximum of tangential stress near tip of a bi-material notch is dependent on the radial distance. In order to mitigate the radial dependence of the maximum in tangential stress, an average value over specific distance d which is fracture mechanism or material microstructure is used.

The criterion of maximum of average tangential stress. The detailed derivation of the equations bellow is found in the dissertation, therefore this sub-chapter presents only the equations in its final form. We can find the crack initiation direction θ_0, where the $\overline{\sigma}_{\theta\theta}\left(\theta\right)$ has its global extreme by solving the equation:

$$\sum_{k=1}^{n} \Gamma_{k1} \frac{d^{\lambda_k}}{\lambda_k} \frac{\partial f_{\theta\theta k}\left(\theta\right)}{\partial \theta} \quad = \quad 0, \tag{7}$$

where the Γ_{k1} is the ratio between individual GSIFs $\Gamma_{k1} = H_k/H_1$. The critical value of GSIF for a notch problem is for complex λ_k and H_k:

$$H_{1\mathrm{C},m} \quad = \quad \frac{K_{\mathrm{IC},m}}{\sqrt{2\pi}\Re\left\{\sum_{k=1}^{n} \Gamma_{k1} \frac{d^{\lambda_k - \frac{1}{2}}}{\lambda_k} f_{\theta\theta k}\left(\theta_{0,m}\right)\right\}}. \tag{8}$$

As introduced by Eq. (6) on p. 8, the generalized fracture toughness $H_{1\mathrm{C},m}$ depends on the fracture toughness $K_{\mathrm{IC},m}$ of the material m. In the case of a bi-material notch, there are two materials in which the crack can initiate. If the value $H_{1\mathrm{C},1}$ is lower than $H_{1\mathrm{C},2}$, crack initiation is expected into the material 1, otherwise it onsets in the material 2. The third option is the crack initiation in the interface. The value $H_{1\mathrm{C,interface}}$ is determined based on fracture toughness of the interface, $K_{\mathrm{IC,interface}}$. Note that for all the critical values $H_{1\mathrm{C},1}$, $H_{1\mathrm{C},2}$ and $H_{1\mathrm{C,interface}}$, the shape functions $f_{\theta\theta k}\left(\theta\right)$ shall contain corresponding angle of potential crack initiation $\theta_{0,m}(m = 1, 2, \mathrm{interface})$. The angle $\theta_{0,m}$ is determined by Eq. (7) for the case when the material contains the global maximum of $\overline{\sigma}_{\theta\theta}\left(\theta\right)$ and equals to γ_2 for the remaining cases of local maximum of $\overline{\sigma}_{\theta\theta}\left(\theta\right)$ of the interface failure. Then, the crack initiation occurs if the following stability criterion is violated [20]:

$$H_1 \quad < \quad \left\{H_{1\mathrm{C},1}, H_{1\mathrm{C},2}, H_{1\mathrm{C,interface}}\right\}. \tag{9}$$

In general, the criteria always compare value H_1 with critical values $H_{1\mathrm{C},m}$. This is true for approach when only the singular terms factors are employed as well as for the multi-parameter approach. There is no need to compute critical values for other terms H_k since they are dependent on H_1 by the ratio Γ_{k1}. Finally the critical load for crack onset from a bi-material notch can be calculated:

$$\sigma_{\mathrm{C}} \quad = \quad \sigma_{\mathrm{appl}} \frac{\min\left(H_{1\mathrm{C},1}\left(\theta_{0,1}\right), H_{1\mathrm{C},2}\left(\theta_{0,2}\right), H_{1\mathrm{C},\mathrm{interface}}\left(\theta_{0,\mathrm{interface}}\right)\right)}{H_1\left(\sigma_{\mathrm{appl}}\right)}. \tag{10}$$

The average strain energy density factor criterion. According to (ii) the mean value of the strain energy density factor Σ, the equation by which we will find the crack initiation angle θ_0 is:

$$\sum_{k=1}^{n}\sum_{l=k}^{n}\Gamma_{k1}\Gamma_{l1}\frac{d^{\lambda_k+\lambda_l-1}}{\lambda_k+\lambda_l}\frac{\partial U_{kl}\left(\theta\right)}{\partial\theta} \quad = \quad 0, \tag{11}$$

where $\Gamma_{l1} = H_l/H_1$. The formula for determination of critical value of GSIF is:

$$H_{1\mathrm{C},m} \quad = \quad K_{\mathrm{IC},m}\sqrt{\frac{k_m}{2\pi\Re\left\{\sum_{k=1}^{n}\sum_{l=k}^{n}\Gamma_{k1}\Gamma_{l1}\frac{d^{\lambda_k+\lambda_l-1}}{\lambda_k+\lambda_l}U_{kl}\left(\theta\right)\right\}}}. \tag{12}$$

Note that all the critical values $H_{1C,1}$, $H_{1C,2}$ and $H_{1\mathrm{C},\mathrm{interface}}$ should be evaluated for calculated corresponding angles of crack initiation $\theta_{0,1}$, $\theta_{0,2}$ and $\theta_{0,\mathrm{interface}}$ respectively, which were determined earlier by Eq. (11). Once the critical fracture toughness values are known, in order to assess stability, the generalized stability condition as stated in equation (6) is used. The condition of stability for the case of a bi-material notch is written identically as in Eq. (9) in the MTS criterion section, since it is a general one. The crack onset load is then calculated by Eq. (10).

Failure load predictions vs. experimental data. Experiments on three point bending specimens made of polymethyl methacrylate (PMMA) with a V-notch were conducted by Dunn et al. in [61]. Dunn et al. tested specimens with notch opening angle 2α of 60°, 90° and 120°. They also varied the notch depth, so the specimens with a/h ratio of 0.1, 0.2, 0.3 and 0.4 were tested. In [61] Dunn et al. measured fracture toughness of PMMA as an average value $K_{\mathrm{IC}} = 1.02$ MPa$\sqrt{\mathrm{m}}$ with standard deviation of 0.12 MPa$\sqrt{\mathrm{m}}$ and the average strength $\sigma_u = 124$ MPa. They reported on failure strength σ_f of notched specimens of individual geometric configuration. We compare their experimental results with our prediction by above mentioned criteria. The $H_{1\mathrm{C},m}$ are determined by Eq. (8) on p. 8 in the case of criterion of maximum of average tangential stress or by Eq. (12) on p. 9 in the case of average strain energy density factor criterion. The generalized fracture toughness is computed by the above stated K_{IC} of PMMA. The crack initiation angle is assumed to be $\theta_0 = 180°$ because of problem symmetry. The parameter d related to microstructure or fracture mechanism was varied, so the charts show predictions with $d = 0.001$ mm, $d = 0.01$ mm and $d = 0.1$ mm. The results for specimens with notch opening angle $2\alpha = 60°$ and $2\alpha = 90°$ are found in Figure 6 and the results for $2\alpha = 120°$ in Figure 7. The review of results show, that the very good agreement between experimental data and theoretical predictions occur for $d = 0.01$ mm especially in the case of the largest opening angle 120°. The use of the above mentioned criteria and parameter $d = 0.01$ mm leads to results which underestimate the actual failure load. From the engineering point of view, it is a desirable situation, since the results lay on so called safe side. The criteria used to predict the failure force are multi-parameter, nevertheless on distances in order of 10^{-2} mm, the contribution of higher order terms is small. The difference in failure loads predicted by the single-parameter criteria and multi-parameter criteria is in units of percents. The higher order terms contribution would become significant for materials and configurations where larger d is necessary.

2.3. Fracture mechanics of sharp material inclusion

The geometry of a bi-material junction as shown in Figure 8 is characterized by angles γ_0, γ_1 and γ_2. Analogically to the case of the sharp notch, complementary opening angle 2α is defined. The joint has two interfaces and no free surface. The material is considered as linear elastic and fully described by Young's moduli and Poisson's ratios in terms of elasticity. Perfect bonding is assumed at the interfaces so the displacements and tractions are assumed to be continuous. The solution mostly presupposes the approximation of plane strain or plane stress. The stress distribution in the case of a bi-material junction is given by the asymptotic expansion [42]:

$$\sigma_{ij}\left(r,\theta\right) \quad = \quad \sum_{k=1}^{\infty}\left\{H_k r^{\lambda_k-1} f_{ijk}(\theta) + \bar{H}_k r^{\bar{\lambda}_k-1}\bar{f}_{ijk}(\theta)\right\}. \tag{13}$$

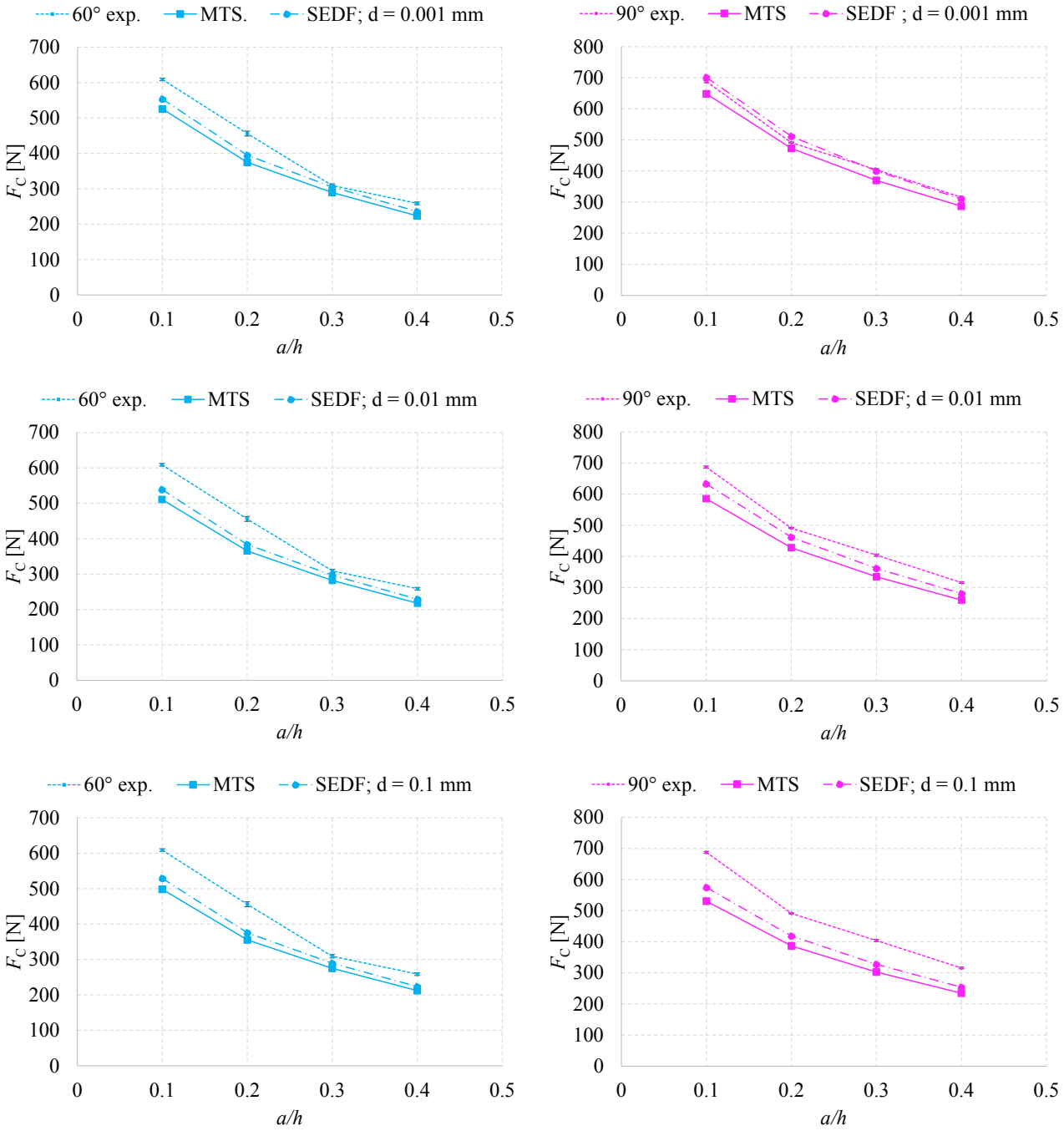

Figure 6: Comparison of experimental failure forces [61], the MTS and SEDF criterion predicted critical forces for a V-notch. The cyan color represents results of $2\alpha = 60°$ and the magenta color represents results of $2\alpha = 90°$.

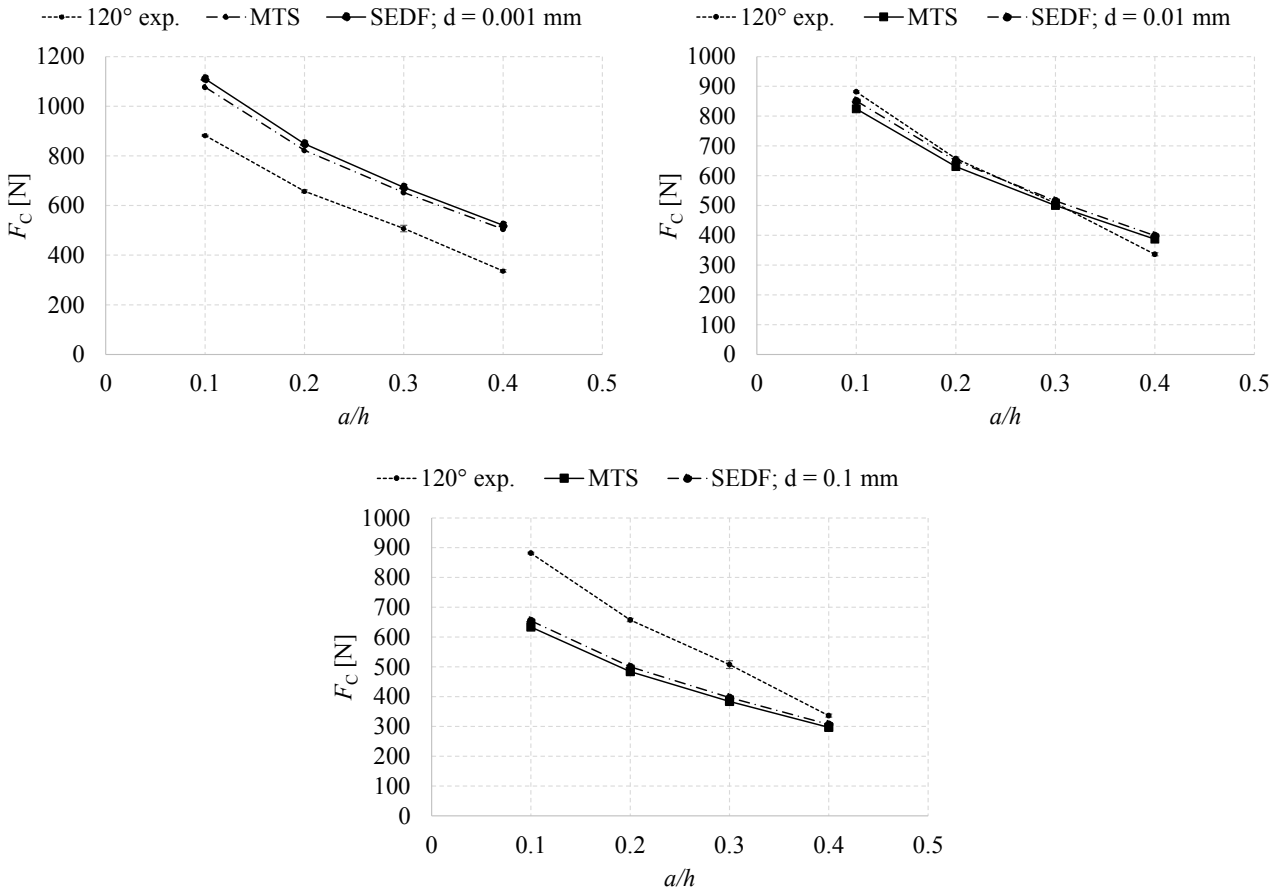

Figure 7: Comparison of experimental failure forces [61], the MTS and SEDF criterion predicted critical forces for a V-notch. Results of $2\alpha = 120°$.

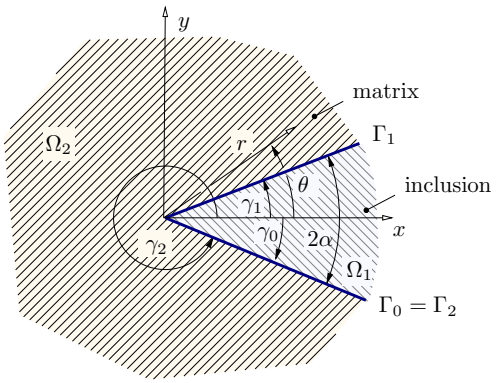

Figure 8: Bi-material junction as a model for a sharp material inclusion.

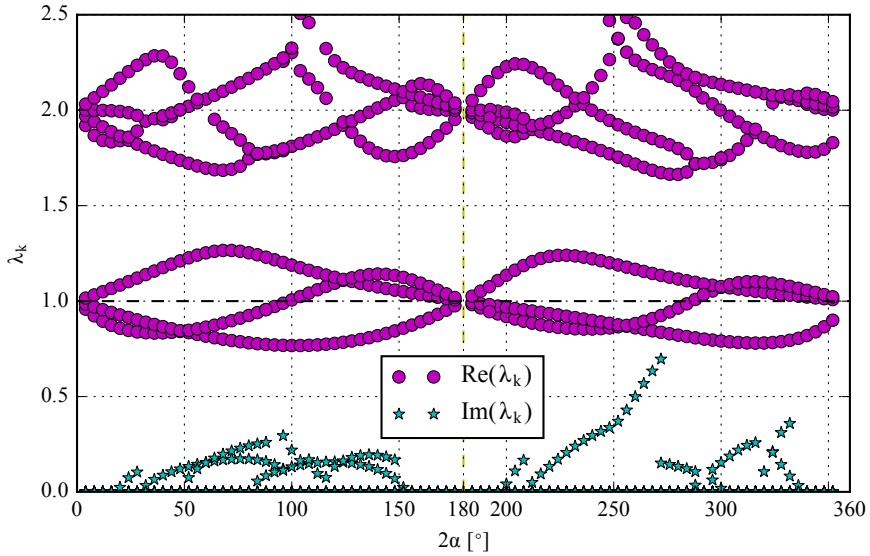

Figure 9: Dependence of eigenvalues λ_k the opening angle 2α. The geometry of the studied bi-material junction is defined: $\gamma_0 = -\alpha$, $\gamma_1 = \alpha$, $\gamma_2 = 2\pi - \alpha$. The Young's moduli ratio is $E_1/E_2 = 0.25$ and Poisson's ratios are $\nu_1 = \nu_2 = 0.25$.

where the indices $(i, j) \equiv (r, \theta)$ are polar coordinates. The symbol H_k again stands for the GSIF. Generally, the eigenvalue λ_k is a complex number. For λ_k satisfying $0 < \Re(\lambda_k) < 1$, the corresponding stress term is considered singular. For λ_k where $1 < \Re(\lambda_k)$ the corresponding stress term is considered non-singular. The boundary conditions of the problem reflect the traction and displacement continuity on both interfaces. Eigenvalue λ_k is found as a solution of the characteristic equation rising from determinant of matrix $\mathbf{A}(\lambda)$ as in the case of a notch. The dependence of eigenvalues for particular bi-material configuration of $E_1/E_2 = 0.25$ is shown in Figure 9. The H_k are determined by methods which are the combination of analytical and numerical approaches such as the Ψ-integral and ODM, as in the case of a notch. However, there are some particular differences in determination of both λ_k and H_k, commented in detail in the dissertation.

Criteria of crack initiation direction and stability criteria

A sharp material inclusion is regarded as a singular stress concentrator, which is represented by a model of a bi-material junction. The mechanism of crack initiation from the bi-material junction tip is presumed to be identical to the mechanism of crack propagation in single homogeneous material. The stability condition of a bi-material junction suggests the condition when the crack is initiated from the bi-material junction tip. Analogical to the case of a V-notch or bi-material notch, the stress singularity exponent changes as the step function during crack initiation. Since an inherently combined loading mode is observed in majority of cases it is generally speaking not possible to separate the modes from each other (possible only in e.g. the symmetrically loaded symmetrical bi-material junction). The stability assessment of a GSSC as it is defined in (6) for a notch can be utilized for the case of a bi-material junction. Then the controlling quantity L regarding the identical physical meaning for a crack in homogeneous material and a bi-material junction has to be chosen.

When we consider sharp rectangular material inclusion, there are 8 possible cases of loading direction and bi-material stiffness ratio variation. This determines the character of singularity, which exists at the singular concentrator tip. These 8 possible configurations are illustrated in Figure 10. For some cases, the singular terms describe the singular solution with solid accuracy (as in Part 1 of the Numerical example on p. 15), in other instances, the employment of higher order terms is essential (as in Part 2 of the Numerical example on p. 18). Let's analyse the configurations with the vertical loading, cases (i)-(iv). The Young's modulus of an inclusion is denoted by E_1 and the modulus of matrix by E_2. The cases (i) and (iii) both act like a V-notch, since the inclusion acts like a compliant reinforcement. In the former case loaded in tension and the latter case in compression. In both cases the singular terms describe the stress state well. Employment of higher order terms increases precision on larger distances from the tip. On the other hand, we have configurations (ii) and (iv) which represent inclusion stiffer than

	inclusion more compliant than matrix ($E_1 < E_2$)			inclusion stiffer than matrix ($E_1 > E_2$)		
loading	case	description by s. t.:	use of n. s. t.:	case	description by s. t.:	use of n. s. t.:
vertical	(i)	good	increased precision	(ii)	poor	necessary
vertical	(iii)	good	increased precision	(iv)	poor	necessary
horizontal	(v)	poor	necessary	(vi)	good	increased precision
horizontal	(vii)	poor	necessary	(viii)	good	increased precision

Table 1: Summary of results, the particular cases are shown in Figure 10. The acronym s. t. stands for singular terms and n. s. t. for non-singular terms.

matrix. The case (ii) is similar to Part 2 of Numerical example, where the stress is not described well by singular terms. The case (iv) is its equivalent in compression, characterized also by poor description of the stress field by singular terms. Employment of higher order terms is essential to obtain stresses that truly represents the stress state near the inclusion tip. The configurations with horizontal tension (v)-(viii) show a different pattern. The cases (v) and (vii), i.e. cases of inclusion more compliant than matrix are characterized by poor stress description by singular terms. To obtain results that represent the actual stress field, employment of higher order terms is necessary. In contrast, in the cases (vi) and (vii) with inclusion stiffer than matrix singular terms describe the stress state well. Again, precision is increased by use of higher order terms. The Table 1 provides a summary of all the cases. The general load of an engineering component is a combined one. Moreover, the orientation of an inclusion in composite is random (depending on the composite type). Therefore, we can not state that the singular terms only are sufficient for the case of an inclusion more compliant than matrix and that the non-singular terms are crucial for the case of inclusion stiffer than matrix. By comparing e.g. the cases (i) and (v) it is obvious, that even for cases of an inclusion more compliant than matrix, the non-singular terms do not describe the stress precisely enough.

The criterion of maximum of average tangential stress

As described in the sub-section 2.2 on p. 8, the maximum tangential stress criterion states that the crack will initiate in the direction of maximal tangential stress. General case of a bi-material junction (non-symmetrical) is characterized by radial dependence of the direction of maximum $\sigma_{\theta\theta}(r,\theta)$. To mitigate this dependence, as in the case of a bi-material notch, we determine the average value of tangential stress $\overline{\sigma}_{\theta\theta}(\theta)$ over some specific distance d. This distance d is established by the relation to microstructure or fracture mechanism. The derivation of the multi-parameter formula to assess stability of a bi-material junction is analogical to the case of a bi-material notch, which is shown in the dissertation. Thus we can rewrite the equation (7):

$$\sum_{k=1}^{n} \Gamma_{k1} \frac{d^{\lambda_k}}{\lambda_k} \frac{\partial f_{\theta\theta k}(\theta)}{\partial \theta} = 0, \tag{14}$$

by which we find the global and local maximum of $\overline{\sigma}_{\theta\theta}(\theta)$. Recall that Γ_{k1} is the ratio between GSIFs defined as $\Gamma_{k1} = H_k/H_1$. In the equation above, the angle of global maximum is the only unknown. In the case of a bi-material junction, there are three possible directions of crack onset. The crack can onset into direction with global maximum of $\overline{\sigma}_{\theta\theta}(\theta)$, into a local maximum, or in one of the interfaces. These three depend on the fracture toughness of inclusion, matrix and the interface, the $K_{\mathrm{IC},1}$, $K_{\mathrm{IC},2}$ and $K_{\mathrm{IC,interface}}$ respectively. Based on an assumption that the crack initiation mechanism is the same as in the case of a crack propagation in homogeneous media, we compute the generalized critical value of fracture toughness as:

$$H_{1\mathrm{C},m} = \frac{K_{\mathrm{IC},m}}{\sqrt{2\pi}\Re\left\{\sum_{k=1}^{n} \Gamma_{k1} \frac{d^{\lambda_k - \frac{1}{2}}}{\lambda_k} f_{\theta\theta k}(\theta_{0,m})\right\}} \tag{15}$$

The generalized fracture toughness of the matrix, inclusion and the interface $H_{1C,1}$, $H_{1C,2}$ and $H_{1\mathrm{C,interface}}$ have to be calculated on corresponding angles of crack onset $\theta_{0,1}$, $\theta_{0,2}$ and $\theta_{0,\mathrm{interface}}$ respectively. The condition of stability is a general one, common for both cases of a bi-material notch and junction, as written in Eq. (9) on p. 8. The critical load is calculated by Eq. (10) on p. 9.

The average strain energy density factor criterion

The strain energy density factor (SEDF) criterion, developed by Sih, found many applications in assessment of

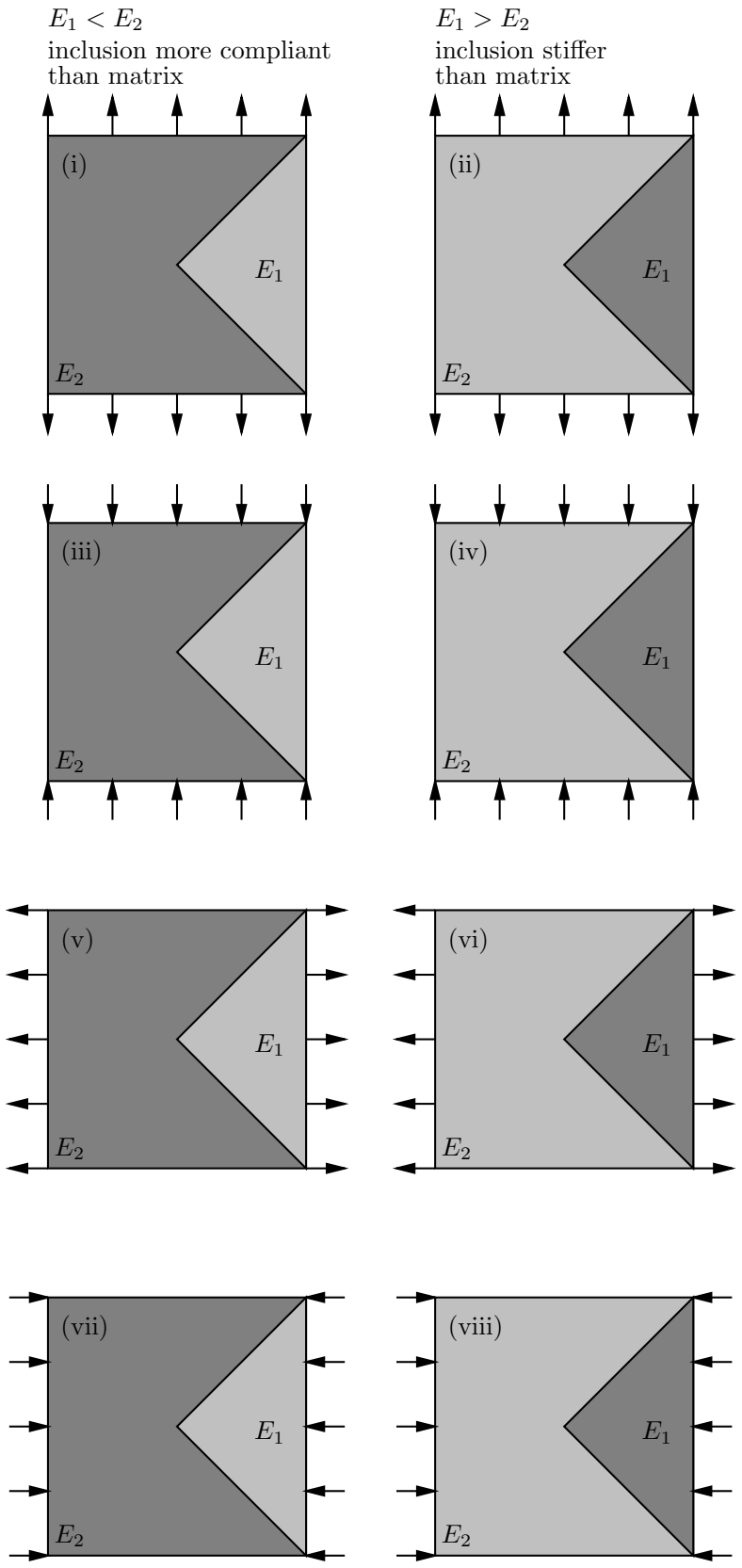

Figure 10: 8 possible cases of rectangular inclusion loading and bi-material variation

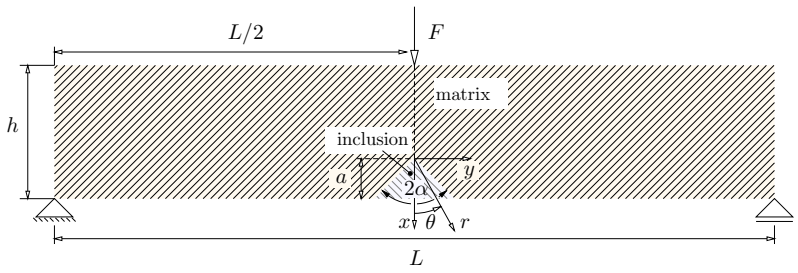

Figure 11: Model of the sharp material inclusion specimen subjected to 3 point bending.

crack problems. The problem of a sharp material inclusion, modeled as a bi-material junction can be assessed by this criterion as well. The theoretical multi-parameter approach is identical to the case of a bi-material notch. The global and local minimum of the SEDF is found as a potential crack initiation direction. Thus we rewrite the formula (11) on p. 9:

$$\sum_{k=1}^{n}\sum_{l=k}^{n}\Gamma_{k1}\Gamma_{l1}\frac{d^{\lambda_k+\lambda_l-1}}{\lambda_k+\lambda_l}\frac{\partial U_{kl}\left(\theta\right)}{\partial\theta} \quad = \quad 0. \tag{16}$$

Based on the SEDF approach, we determine the generalized fracture toughness for all potential crack onset directions, the global minimum, local minimum and the interface. This is achieved by Eq. (12) on p. 9, written as:

$$H_{1\mathrm{C},m} \quad = \quad K_{\mathrm{IC},m}\sqrt{\frac{k_m}{\pi\Re\left\{\sum_{k=1}^{n}\sum_{l=k}^{n}\Gamma_{k1}\Gamma_{l1}\frac{d^{\lambda_k+\lambda_l-1}}{\lambda_k+\lambda_l}U_{kl}\left(\theta\right)\right\}}}. \tag{17}$$

The condition of stability is a general one, common to all general singular stress concentrators, stated in Eq. (9) on p. 8. Finally the formula for critical load, also a general one, is given by Eq. (10) on p. 9.

Numerical example: Crack initiation direction and initiation load in the case of a bi-material junction

Part 1 Let's consider a problem shown in Figure 11, which represents a three point bending specimen with rectangular inclusion. In the Part 1 we consider inclusion more compliant than matrix where $E_1/E_2 = 0.033$. The material region 1, which represents the inclusion, is modeled with PMMA material properties $E_1 = 2.3$ GPa, $\nu_1 = 0.34$ and the material region 2, which represents matrix, with aluminum material model characterized by $E_2 = 69$ GPa, $\nu_2 = 0.33$. To assess crack initiation direction we use (a) criterion of maximum of average tangential stress and (b) average strain energy density criterion. The fracture toughness of PMMA is $K_{\mathrm{IC}}^{\mathrm{PMMA}} = 1.02$ MPa$\sqrt{\mathrm{m}}$ [61]. The fracture toughness of aluminum is $14 \div 28$ MPa$\sqrt{\mathrm{m}}$ depending on the particular alloy and treatment. We choose aluminum alloy (7075) with $K_{\mathrm{IC}}^{\mathrm{Al}} = 24$ MPa$\sqrt{\mathrm{m}}$. Without an experiment with the particular bi-material configuration, it is uneasy to estimate fracture toughness of the interface. In [62] Shatil and Shaimoto tested aluminum/PMMA bi-material 3PB specimens, however they do not provide value regarding fracture toughness of the interface. To bond the materials together they use epoxy adhesive. Experimental evaluation in [64, 63] show that the fracture toughness of interface can vary widely depending on conditions and particular configuration of materials to be bonded. Our estimation for this numerical example therefore is $K_{\mathrm{IC}}^{\mathrm{interface}} = 0.75$ MPa$\sqrt{\mathrm{m}}$.

(a) The criterion of maximum of average tangential stress. The tangential stress is averaged over a specific distance d, which is chosen as 1 mm. The averaged tangential stress calculated by (i) singular terms (the yellow dotted line) and by (ii) singular and non-singular terms (the cyan dotted line) is shown in Figure 12. The yellow line with markers represents the solution of $\sigma_{\theta\theta}\left(r,\theta\right)$ on $d = 1$ mm by singular terms. In similar manner, the cyan line with markers represents the singular and non-singular terms solution. For this particular bi-material and geometrical configuration there are two singular terms. Regarding the singular and non-singular terms solution,

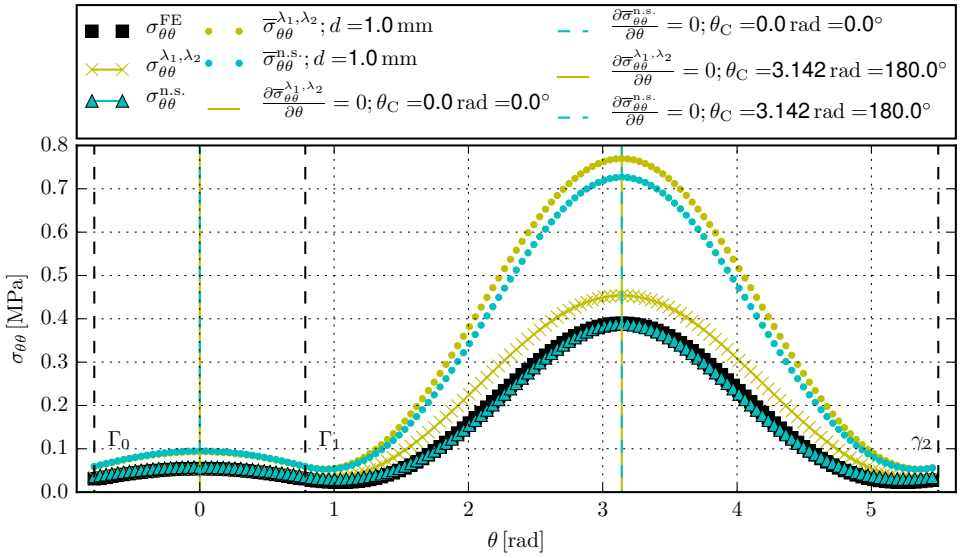

Figure 12: Average value of the $\overline{\sigma}_{\theta\theta}(\theta)$ plotted by (i) singular terms: the yellow line, by (ii) singular and non-singular terms: the cyan line. The black dashed lines denote the interfaces.

two singular and two non-singular terms are considered. Please recall the formula to find potential crack initiation directions (14) on p. 13. We see that there are two extremes in the tangential stress angular distribution, the global maximum (occurs in the matrix, $m = 2$) and the local maximum (occurs in the inclusion, $m = 1$). In both cases, the singular terms solution of extreme (represented by the vertical yellow solid line) and the non-singular terms solution of extreme (represented by the vertical cyan dashed line) has the same direction (both in the local and global average tangential stress maximum). The potential crack initiation direction in the global maximum is $\theta_0^{\mathrm{glb.}} = 180°$ and in local maximum $\theta_0^{\mathrm{loc.}} = 0°$ which is apparent because of the problem symmetry. Nevertheless, as the solution by employment of non-singular terms is more precise, increase in precision of the critical parameters is also expected. In the previous theoretical chapter we stated that the crack initiation can occur in the inclusion, matrix or the interface, whereas each of them possesses a particular material parameter $K_{1\mathrm{C},m}$ and therefore different $H_{1\mathrm{C},m}$. We calculate these critical values by Eq. (15). The results (i) singular terms solution are found in Table 2 and results of (ii) non-singular terms solution in Table 3. The methods (i) and (ii) lead to difference of 5.94 % in $H_{1\mathrm{C},2}$ which is in global maximum, 1.72 % in $H_{1\mathrm{C},1}$ which is in local maximum and 0.83 % in interface critical GSIF value. The minimum value of $H_{1\mathrm{C},m}$ is found in the PMMA. By criterion of maximum of average tangential stress the crack is therefore predicted to initiate in this direction and material. Remember, that we assume interface with perfect adhesion, which allows full traction transmission. If the actual interface does not comply to this assumption and crack may not initiate in this predicted direction.

	$\theta_{0,m}$	m	$H_{1\mathrm{C},m}$
global maximum	180.0°	2 ≡ aluminum	177.765048
local maximum	0.0°	1 ≡ PMMA	62.32677
interface	±45.0°	interface	72.968331

Table 2: The generalized fracture toughness $H_{1\mathrm{C},m}$ for global minimum, local minimum and the interface determined by (i) singular terms and (a) criterion of maximum of average tangential stress.

	$\theta_{0,m}$	m	$H_{1\mathrm{C},m}$
global maximum	180.0°	2 ≡ aluminum	188.317388
local maximum	0.0°	1 ≡ PMMA	61.254716
interface	±45.0°	interface	72.359732

Table 3: The generalized fracture toughness $H_{1\mathrm{C},m}$ for global minimum, local minimum and the interface determined by (ii) singular and non-singular terms and (a) criterion of maximum of average tangential stress.

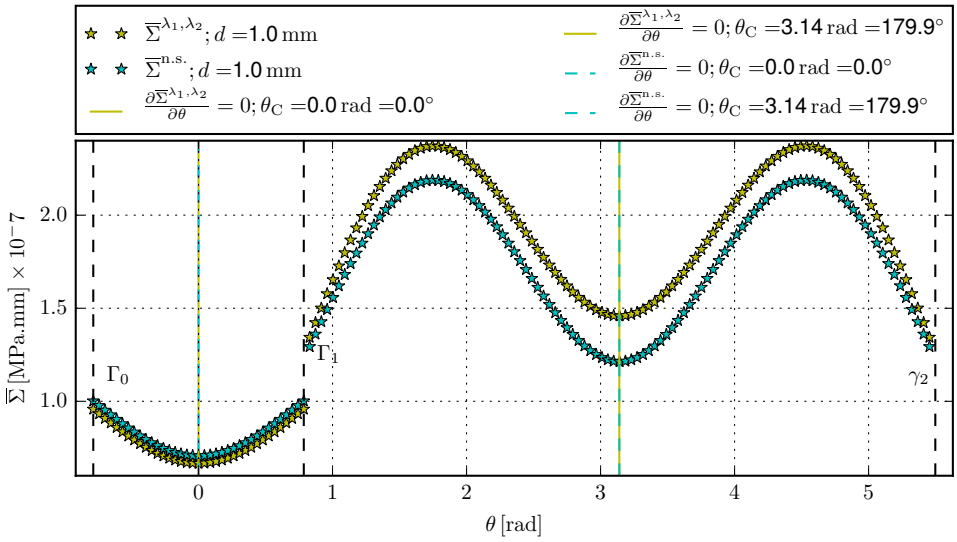

Figure 13: Average value of the $\overline{\Sigma}(\theta)$ plotted by (i) singular terms: the yellow line, by (ii) singular and non-singular terms (the cyan line). The black dashed lines denote the interfaces.

(b) The average strain energy density factor criterion. The averaged strain energy density factor over distance $d = 1$ mm is plotted in Figure 13. The yellow line represents solution by (i) two singular terms and the cyan line represents solution by (ii) two singular and two non-singular terms. We see that there is a global minimum and a local one, found by solving Eq. (16). Both (i) and (ii) return identical angular values corresponding to these points. However some offset of $\overline{\Sigma}(\theta)$ between solutions exists, therefore difference in critical parameters is expected. The generalized fracture toughnesses are calculated by formula (17). The results (i) singular terms solution are found in Table 4 and results of (ii) non-singular terms solution in Table 5. The methods (i) and (ii) leads to the difference of 9.6 % in $H_{1\mathrm{C},2}$ which corresponds to local minimum, 2.9 % in $H_{1\mathrm{C},1}$ for global minimum and 2.2 % in interface critical GSIF value prediction. The lowest value of generalized fracture toughness corresponds to the interface, thus the crack is expected to initiate in this direction. We see that the crack initiation direction and material predicted by (a) and (b) is different as in the former case the crack is predicted to initiate in PMMA with $\theta_0^{\mathrm{glb.}} = 0°$ and the latter case it is predicted to initiate in the interface with $\theta_{0,\mathrm{interface}} = \pm 45°$. In (a) only the tangential stress component is used to calculate $H_{1\mathrm{C},m}$ whereas in (b) all stress components are employed. The level of tangential stress acting on the interfaces is low, leading to higher value of $H_{1\mathrm{C},\mathrm{interface}}$ calculated by (a) than by (b).

	$\theta_{0,m}$	m	$H_{1\mathrm{C},m}$
global minimum	0.0°	1 ≡ PMMA	62.786943
local minimum	179.9°	2 ≡ aluminum	187.279553
interface	±45.0°	interface	39.704644

Table 4: The generalized fracture toughness $H_{1\mathrm{C},m}$ for global minimum, local minimum and the interface determined by (i) singular terms and (b) average strain energy density criterion.

	$\theta_{0,m}$	m	$H_{1\mathrm{C},m}$
global minimum	0.0°	1 ≡ PMMA	60.974337
local minimum	179.9°	2 ≡ aluminum	205.32978
interface	±45.0°	interface	38.813687

Table 5: The generalized fracture toughness $H_{1\mathrm{C},m}$ for global minimum, local minimum and the interface determined by (ii) singular and non-singular terms and (b) average strain energy density criterion.

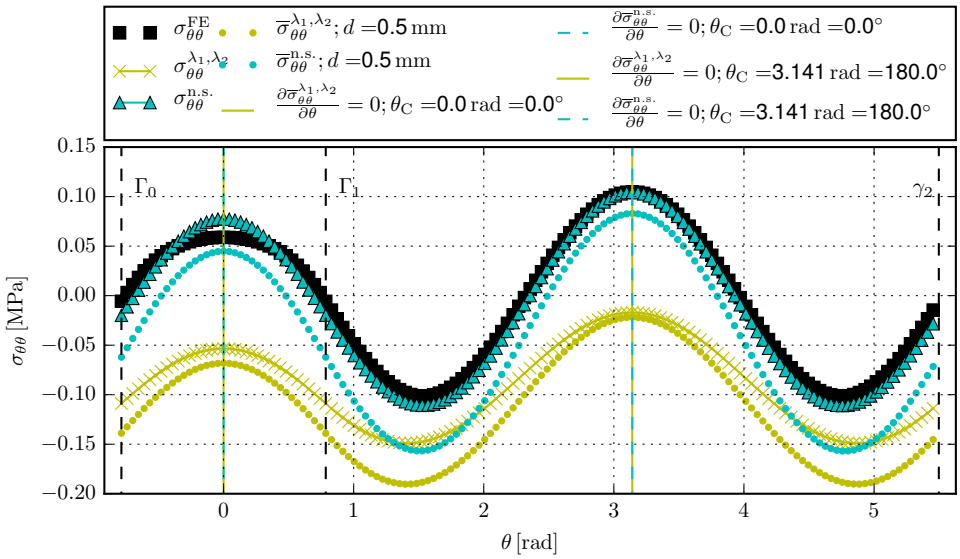

Figure 14: Average value of the $\sigma_{\theta\theta}^{-}(\theta)$ plotted by (i) singular terms: the yellow line, by (ii) singular and non-singular terms (the cyan line). The black dashed lines denote the interfaces.

Part 2 In the Part 2 we consider three point bending specimen with rectangular inclusion stiffer than matrix where $E_1/E_2 = 30$. The elastic constants remain identical to those in Part 1, only the inclusion is modeled with aluminum material properties and the matrix with PMMA material properties. Again, to assess crack initiation direction and critical value of GSIF we use (a) the criterion of maximum of average tangential stress and (b) the average strain energy density criterion. In the part 2 of the numerical example, we use averaging distance $d = 0.5$ mm.

(a) The criterion of maximum of average tangential stress. The distribution of $\overline{\sigma}_{\theta\theta}(\theta)$ is shown in Figure 14, where the yellow dotted line represents the averaged tangential stress solution given by (i) two singular terms. The cyan line represents the solution given by (ii) two singular and two non-singular terms. In addition, the stress on particular distance d is plotted by (i) and (ii) and denoted by lines with markers. Please note that the tangential stress given by (i) is compressive for all θ. The black squares represents the FE solution. As in the previous case, we see two extremes of $\overline{\sigma}_{\theta\theta}(\theta)$ represented by vertical lines, the yellow in case of (i) and the cyan in case of (ii). Both singular and non-singular solution predict identical angles of crack initiation, i. e. $\theta_0^{\mathrm{glb.}} = 180°$ and $\theta_0^{\mathrm{loc.}} = 0°$. The difference in stress description by (i) and (ii) is severe, therefore significant difference in value of critical parameters is expected. The results by (i) are listed in Table 6. The results given by (ii) is summarized in Table 7. When (i) only the singular terms are taken as an input for critical GSIF calculation a negative valued $H_{1\mathrm{C},m}$ are obtained (since the $\overline{\sigma}_{\theta\theta}(\theta)$ is compressive). For (ii), the minimum value is $H_{1\mathrm{C},2}$ and the crack is expected to initiate in the direction of global maximum found in PMMA.

	$\theta_{0,m}$	m	$H_{1\mathrm{C},m}$
global maximum	180.0°	2 ≡ PMMA	(-0.015640)
local maximum	0.0°	1 ≡ aluminum	(-0.117511)
interface	±45.0°	interface	(-0.001800)

Table 6: The generalized fracture toughness $H_{1\mathrm{C},m}$ for global minimum, local minimum and the interface determined by (i) singular terms and (a) criterion of maximum of average tangential stress.

	$\theta_{0,m}$	m	$H_{1\mathrm{C},m}$
global maximum	180.0°	2 ≡ PMMA	0.004104
local maximum	0.0°	1 ≡ aluminum	0.178545
interface	±45.0°	interface	(-0.004031)

Table 7: The generalized fracture toughness $H_{1\mathrm{C},m}$ for global minimum, local minimum and the interface determined by (ii) singular and non-singular terms and (a) criterion of maximum of average tangential stress.

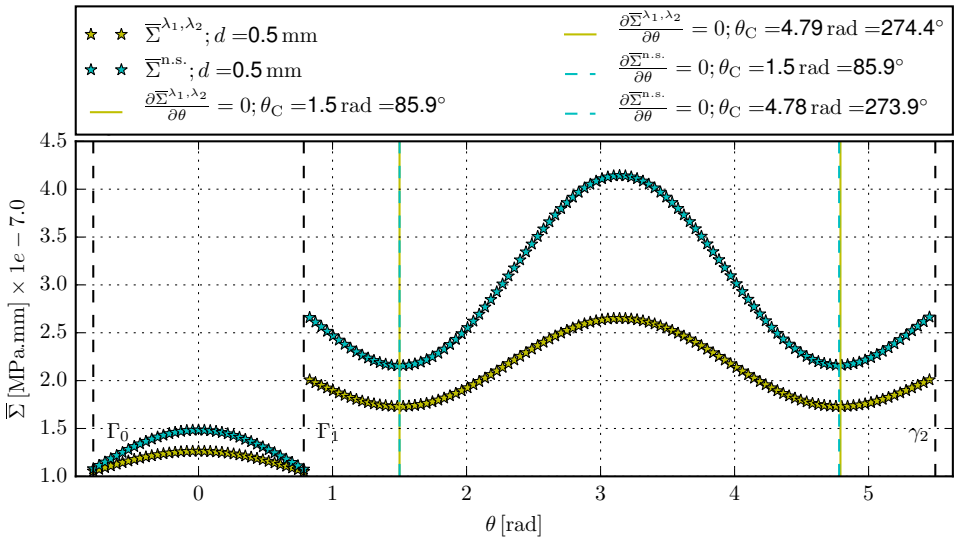

Figure 15: Average value of the $\bar{\Sigma}(\theta)$ plotted by (i) singular terms: the yellow line, by (ii) singular and non-singular terms: the cyan line. The black dashed lines denote the interfaces. In the region of inclusion, i.e. the $\bar{\Sigma}(\theta)$ is multiplied by factor of 10.

(b) The average strain energy density factor criterion. The angular distribution of strain energy density factor $\overline{\Sigma}(\theta)$ is shown in Figure 15. The yellow line represents (i) two singular terms solution. The cyan line represents (ii) two singular and two non-singular terms solution. Because the problem is a symmetric one, there are two directions where global minimum and local minimum are found. The yellow and cyan vertical lines represent the locations of local minima. The global minima are found at the interfaces. The results by (i) are listed in Table 8 and by (ii) in Table 9. The results by (i) are listed in Table 8. The results given by (ii) is summarized in Table 9.The difference in $H_{1\mathrm{C},m}$ by (i) and (ii) is 1.1 % for the global minimum, 10.7 % for local minimum and 1.1 % for the interface. The lowest value of $H_{1\mathrm{C},m}$ is found at the interface, therefore it is the expected angle of crack initiation. The angle and material of expected crack initiation is different from (a), but as discussed in first part of this example, the possible explanation is that the SEDF uses all the stress components rather than tangential stress only. The thorough explanation of such behavior will be a subject of following research as well as experimental evaluation of the problem.

	$\theta_{0,m}$	m	$H_{1C,m}$
global minimum	±45.0°	1 ≡ aluminum	0.027674
local minimum	85.9°, 274.4°	2 ≡ PMMA	0.001334
interface	±45.0°	interface	0.000865

Table 8: The generalized fracture toughness $H_{1C,m}$ for global minimum, local minimum and the interface determined by (i) singular terms and (b) average strain energy density criterion.

	$\theta_{0,m}$	m	$H_{1C,m}$
global minimum	±45.0°	1 ≡ aluminum	0.027360
local minimum	85.9°, 273.9°	2 ≡ PMMA	0.001477
interface	±45.0°	interface	0.000855

Table 9: The generalized fracture toughness $H_{1C,m}$ for global minimum, local minimum and the interface determined by (ii) singular and non-singular terms and (b) average strain energy density criterion.

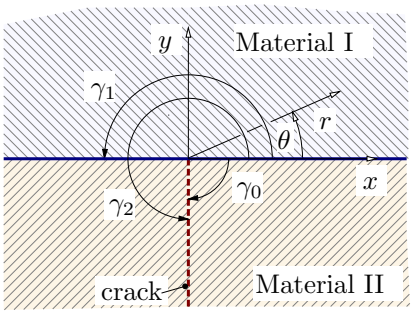

Figure 16: Crack terminating at the inclusion/matrix interface.

Developing a complete description of crack initiation and propagation near the sharp material inclusion

This chapter examines possible scenarios of crack behavior near the sharp material inclusion embedded in matrix. Crack in matrix terminating at inclusion/matrix interface is shown left-hand side of Figure 17. Similarly, the crack in inclusion terminating at the inclusion/matrix interface is shown in right-hand side of Figure 17. This case can be modeled as a crack with its tip at a bi-material interface. The geometry of problem is shown in Figure 16. The crack that terminated at the interface can either propagate to the other material or propagate through the inclusion/matrix interface. The latter situation is examined further in Figure 18, where crack propagating through the inclusion/matrix interface is shown. In the left-hand side of the Figure 18 the crack originates in matrix and in the left-hand side of the Figure 18 it originates in inclusion. These cases is modeled as interfacial cracks (special case of the bi-material notch model with $2\alpha = 0°$ and e.g. $\gamma_1 = 0°$, $\gamma_2 = 180°$ and $\gamma_3 = 360°$. Another situation occurs when the crack reaches the end point of the sharp material inclusion, as shown in Figure 19 (another special case of the bi-material notch model with $2\alpha = 0°$ and e.g. $\gamma_1 = 0°$, $\gamma_2 = 270°$ and $\gamma_3 = 360°$). Figure 20 shows crack initiated at the tip of the sharp material inclusion in the matrix (left-hand side) or in the inclusion (right-hand side). This case is modeled as a bi-material junction. Above mentioned situations capture complete crack behavior near the sharp material inclusion and all can be modeled by methods described in the dissertation.

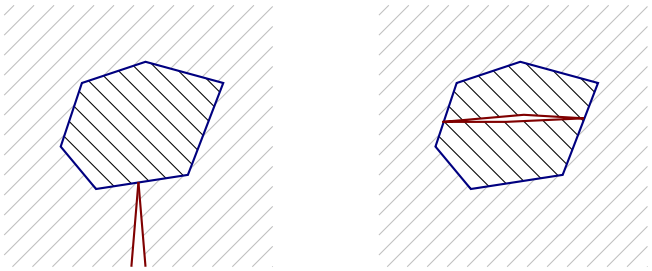

Figure 17: Crack terminating at the inclusion/matrix interface. On the left-hand side the crack originates in matrix. On the right-hand side the crack originates in the inclusion.

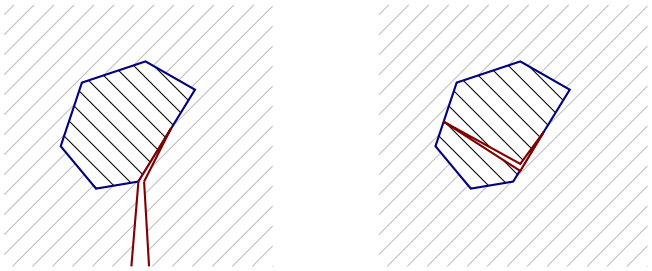

Figure 18: Crack propagating through the inclusion/matrix interface. On the left-hand side the crack originates in matrix. On the right-hand side the crack originates in the inclusion.

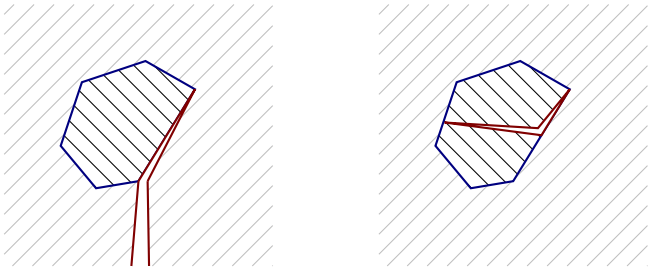

Figure 19: Crack propagated to the end point of inclusion/matrix interface. On the left-hand side the crack originates in matrix. On the right-hand side the crack originates in the inclusion.

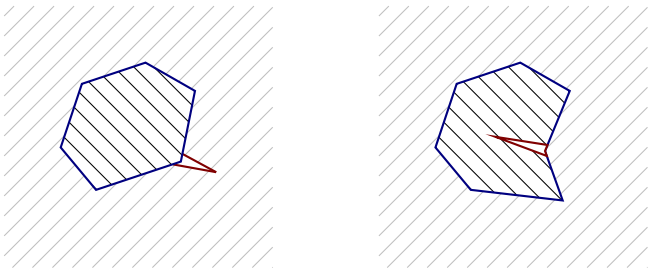

Figure 20: Crack initiated at the tip of the sharp material inclusion. On the left-hand side the crack initiates in matrix. On the right-hand side the crack initiates in matrix.

3. Conclusions

Methods of the classical fracture mechanics can not be directly applied on general singular stress concentrators and its generalization is the current objective of many researchers. The identical motivation stays behind this thesis. Although the dissertation is primarily theoretical, it provides the researchers with the framework in order to fully assess generalized singular stress concentrators in terms of the multi-parameter criteria proposed herein. Experiments to verify the theory on general singular stress concentrators different from a V-notch are the next step to be conducted. For this purpose the specimens modeled in this work can be used.

The dissertation presents methods to determine the eigenvalues to form the exponents of singular and non-singular stress terms in cases of general singular stress concentrators. When the eigenvalues are determined, the angular eigenfunction can be easily formed. The cases of a V-notch, bi-material notch and bi-material junction are studied in detail. However, the methods presented herein allow researchers to determine the order of singularity for any type of multi-material general singular stress concentrator (for example quad-material notch or quad-material junction). In the following part, application of two different methods to determine generalized stress intensity factors of singular and non-singular terms are studied. The main advantage of the Ψ-integral method is, that it allows independent determination of kth generalized stress intensity factor. The overdeterministic method is simpler and computationally less expensive. When some requirements are fulfilled, i.e. if the integration path is far enough from singular point in the case of the Ψ-integral, or number of terms n to be determined is high enough in the case of the ODM, both methods return results very close to each other. By the knowledge of the eigenvalues and generalized stress intensity factors, stress field near singular point can be reconstructed. The analytical solution can be compared with pure finite element solution. When we are interested in the stress field on distances such as $0.1 - 1$ mm, the employment of non-singular terms leads either to significant increase in precision (notches and inclusion more compliant than matrix) or provides the only means to describe the stress field well (inclusion stiffer than matrix).

The dissertation also presents stability criteria modified to contain higher order terms. These multi-parameter criteria are namely the criterion of maximum of average tangential stress and the average strain energy density factor criterion. Both criteria are applied on problems of V-notch, bi-material notch and bi-material junction. In the case of V-notch, comparison of the predicted failure loads and experimental data show very good agreement. In other cases, the crack initiation direction and critical parameters are calculated. Use of the multi-parameter criteria leads to change in the predicted critical parameters in order of percents. The experimental validation of proposed criteria will be a subject of further research.

4. Selected references of the dissertation

[1] Pook, L. *Linear elastic fracture mechanics for engineers: theory and applications.* Boston: WIT Press, 2000, 154 p. ISBN1853127035.

[2] Anderson, T.L. *Fracture mechanics: fundamentals and applications.* Second Edition. Boca Raton: CRC Press, 1995, 669 p. ISBN 0849342600.

[3] Sun, C., Jin J. *Fracture mechanics.* Waltham, MA: Academic Press, 2012, xvii, 311 p. ISBN0123850010.

[4] Muskhelishvili N.I. *Some Basic Problems of the Mathematical Theory of Elasticity*, Noordhoff, Groningen, 1953.

[5] England, A.H. *Complex Variable Methods in Elasticity*, Donver Publications, New York, 2003.

[6] Kaw, A.K. *Mechanics of composite materials.* 2nd ed. Boca Raton, FL: Taylor & Francis, 2006, 466 p. Mechanical engineering series (Boca Raton, Fla.), v. 29. ISBN 9780849313431.

[7] Hwu, Ch. *Anisotropic Elastic Plates*, Spinger, Verlag US, 2010, 673 p. ISBN 978-1-4419-5914-0.

[8] Williams, M.L., Stress singularities resulting from various boundary conditions in angular corners of plates in extensions, Journal of Applied Mechanics 19 (1952) 526 – 528.

[9] Williams, M.L, On the Stress Distribution at the Base of Stationary Crack, Journal of Applied Mechanics, 24 (1957) 109-114.

[10] Hein, V.L., Erdogan, F., Stress Singularities in a Two-Material Wedge, International Journal of Fracture Mechanics 7 (1971) 317-330.

[11] Paris, P.C., Erdogan, F. A critical analysis of crack propagation laws, Journal of Basic Engineering, ASME, 85 (1963) 528-534.

[12] Hutař, P., Seitl, S., Knésl, Z. Quantification of the effect of specimen geometry on the fatigue crack growth response by two-parameter fracture mechanics, Materials Science and Engineering 387–389 (2004) 491-494.

[13] Tong, J., T-stress and its implications for crack growth, Engineering Fracture Mechanics 69 (2002) 1325–1337.

[14] Seitl, S., Knésl, Z., Two parameter fracture mechanics: Fatigue crack behavior under mixed mode conditions, Engineering Fracture Mechanics 75 (2008) 857-865.

[15] Moon, H.J., Earmme, Y.Y., Calculation of elastic T stresses near interface crack tip under in-plane and antiplane loading, Int. J. Fracture 91 (1998) 179-195.

[16] Kotousov, A., On stress singularities at angular corners of plates of arbitrary thickness under tension, International Journal of Fracture 132 (2005) 29-36.

[17] Klusák, J., Profant, T., Kotoul, M., Study of the stress distribution around an orthotropic bi-material notch tip, Key Engineering Materials 417-418 (2010) 385-388.

[18] Klusák, J., Knésl, Z., Reliability assessment of a bi-material notch: Strain energy density factor approach, Theoretical and Applied Fracture Mechanics 53 (2010) 89-93.

[19] Klusák, J., Profant, T., Kotoul, M., Determination of the threshold values of orthotropic bi-material notches, Procedia Engineering 2 (2010) 1635–1642.

[20] Klusák, J., Profant, T., Knésl, Z., Kotoul, M., The influence of discontinuity and orthotropy of fracture toughness on conditions of fracture initiation in singular stress concentrators, Engineering Fracture Mechanics 110 (2013) 438–447.

[21] Krepl, O., Klusák, J., Reconstruction of a 2D stress field around the tip of a sharp material inclusion, Procedia Struct. Integrity 2 (2016) 1920–1927.

[22] Krepl, O., Klusák, J., The influence of non-singular terms on the precision of stress description near a sharp material inclusion tip, Theoretical and Applied Fracture Mechanics 90 (2017) 85-99.

[23] Leguillon, D., Strength or toughness? A criterion for crack onset at a notch, European Journal of Mechanics A/Solids 21 (2002) 61–72.

[24] Leguillon, D., Calcul du taux de restitution de l'énergie au voisinage d'une singularité. C. R. Acad. Sci. Paris Sér. II 309 (1989) 945–950.

[25] Leguillon, D., Asymptotic and numerical analysis of a crack branching in non-isotropic materials, Eur. J. Mech. A Solids 12 (1993) 33-51.

[26] Erdogan, F., Sih, G.C., On the crack extension in plates under plane loading and transverse shear, Int. J. Basic Engineering 85 (1963) 519 – 527.

[27] Ayatollahi, M. R., Dehghany, M., On T-stresses near V-notches, Int. J. Fract. 165 (2010) 121–126.

[28] Náhlík, L., Knésl, Z., Klusák, J.: Crack initiation criteria for singular stress concentrations, Part III: An Application to a Crack Touching a Bimaterial Interface, Engineering Mechanics 15 (2008) 99 – 114.

[29] Qian, Z.Q., Akisania, A.R., Wedge corner stress behaviour of bonded dissimilar materials, Theoretical and Applied Fracture Mechanics 32 (1999) 209-222.

[30] Dundurs, J., Effect of elastic constants on stress in composite under plane deformation, Journal of Composite Materials 1 (1967) 310-322.

[31] Seweryn, A. Molski, K., Elastic stress singularitiesand corresponding generalized stress intensity factors for angular corners under various boundary conditions, Engineering Fracture Mechanics 55 (1996) 529-556.

[32] Klusák, J., Knésl, Z., Náhlík, L., Crack initiation criteria for singular stress concentrations, Part II: Stability of sharp and bi-material notches, Engineering mechanics, Vol. 14, 2007, 6, p. 409-422.

[33] Profant T., Ševeček O., Kotoul M., Calculation of K-factor and T-stress for cracks in anisotropic bimaterials, Engineering Fracture Mechanics 75 (2008) 3707-3726.

[34] Seweryn, A., Modeling of singular stress fields using finite element method, International Journal of Solids and Structures 39 (2002) 4787-4804.

[35] Ayatollahi, M.R., Nejati, M., An over-deterministic method for calculation of coefficients of crack tip asymptotic field from finite element analysis, Fatigue and Fracture of Engineering Materials and Structures 34 (2010) 159-176.

[36] Ayatollahi, M.R., Nejati, M., Determination of NSIFs and coefficients of higher order terms for sharp notches using finite element method, International Journal of Mechanical Sciences 53 (2011) 164–177.

[37] Hilton, P.D., Sih, G.C., Applications of the finite element method to the calculations of stress intensity factors, 1973. In: Sih., G. C., Mechanics of Fracture – Methods of analysis and solutions of crack problems, Noordhoff International Publishing, Leyden, 426-477.

[38] Owen D.R.J, Fawkes A.J., *Engineering Fracture Mechanics: Numerical Methods and Applications.* Pineridge Press Ltd, Swansea, 1983.

[39] Vu-Quoc, L., Tran, V.-X.: Singular analysis and fracture energy-release rate for composites: Piecewise homogenous-anisotropic materials, Comput. Methods Appl. Mech. Eng. 195 (2006) 5162–5197.

[40] Knésl, Z.: A criterion of V-notch stability. International Journal of Fracture 48 (1991) 79-83.

[41] Knésl, Z., Klusák, J. Náhlík, L., Crack initiation criteria for singular stress concentrations, Part I: A universal assessment of singular stress concentrations, Engineering Mechanics 14 (2007) 399-408.

[42] Pageau, S., Joseph, P., Biggers S.: The order of stress singularities for bonded and disbonded three-material junctions, Int. J. Solid Structures 31 (1994) 2979-2997.

[43] Paggi, M., Carpinteri, A., On the stress singularities at multimaterial interfaces and related analogies with fluid dynamics and diffusion, Appl. Mech. Rev. 61 (2008) 1–22.

[44] Yang, Y., Munz D., Stress Intensity Factor and stress distribution in a joint with an interface corner under thermal and mechanical loading, Computers & Structures 57 (1995) 467 – 476.

[45] Larsson, S.G. and Carlsson, A.J., Influence of non-singular stress terms and specimen geometry on small scale yielding at crack tips in elastic-plastic materials, Journal of the Mechanics and Physics of Solids 21 (1973) 263-277.

[46] Bétegon, C., Hancock, J.W., Two-parameter characterization of elastic-plastic crack-tip fields, Journal of Applied Mechanics 58 (1991) 104–110.

[47] Ayatollahi, M.R., Pavier, M.J. and Smith, D.J. Mode I cracks subjected to large T-stresses, International Journal of Fracture 117 (2002) 159-174.

[48] Cotterell, B, Rice, J.R. Slightly curved or kinked cracks, International Journal of Fracture 16 (1980) 155-169.

[49] Kfouri, A. P., Some evaluations of the elastic T-term using Eshelby's method, Int. J. Fracture 30 (1986) 301-315.

[50] Sládek, J., Sládek, V., Evaluations of the T-stress for interface cracks by the boundary element method, Engineering Fracture Mechanics 56 (1997) 813-825.

[51] Profant, T., Ševeček, O., Kotoul, M., Calculation of K-factor and T-stress for cracks in anisotropic bimaterials, Engineering Fracture Mechanics 75 (2008) 3707-3726.

[52] Kim, J.K., Cho, S.B., Effect of second non-singular term of mode I near the tip of a V-notched crack, Fatigue and Fracture of Engineering Materials and Structures 32 (2009) 346-356.

[53] Ayatollahi, M.R., Dehghany, M., Nejati, M., Fracture analysis of V-notched components – Effects of first non-singular stress term, Int. J. Solids Struct. 48 (2011) 1579-1589.

[54] Ayatollahi, M.R., Mirsayar, M.M., Dehghany, M., Experimental determination of stress field parameters in bi-material notches using photoelasticity, Materials and Design 32 (2011) 4901–4908.

[55] Ayatollahi, M.R., Mirsayar, M.M., Nejati, M.: Evaluation of first non-singular stress term in bi-material notches, Computational Materials Science 50 (2010) 752–760

[56] Farris, F.A. (2017). Visualizing complex-valued functions in the plane | Mathematical Association of America. [online] Maa.org. Available at: https://www.maa.org/visualizing-complex-valued-functions-in-the-plane [Accessed 22 Nov. 2017].

[57] Sih, G.C., A special theory of crack propagation, in: G. C. Sih (Ed.), Mechanics of Fracture - Methods of analysis and solutions of crack problems, Noordhoff Internation Publishing, Leyden, The Netherlands, 1973, pp. XXI-XLV.

[58] Sih, G.C., Mechanics of Fracutre Initiation and Propagation, Kluwer Academic Publishing, Boston, 1991.

[59] Taylor, D., The theory of critical distances, Engineering Fracture Mechanics 75 (2008) 1696–1705

[60] Plane Stress and Plane Strain Analysis (2017) College of Engineering - UC Santa Barbara. [online]. Available at: https://engineering.ucsb.edu/~hpscicom/projects/stress/introge.pdf [Accessed 22 Nov. 2017].

[61] Dunn, M.L., Suwito, W., Cunningham, S., Fracture initiation at sharp notches: correlation using critical stress intensities, Int. J. Solid Structures. 34 No. 29 (1997) 3873-3883.

[62] Shatil, G., Saimoto A., Ductile-Brittle Fatigue and Fracture Behaviour of aluminium/PMMA Bimaterial 3PB Specimens, Gruppo Frattura [online]. Available at: http://www.gruppofrattura.it/pdf/cp/cp2006/78.pdf [Accessed 22 Nov. 2017].

[63] Bo, Z., Jing-wei, L., Shu-guang, L., Yi-hui, L., Ju-tau, H., Relationship between fracture toughness and temperature in epoxy coatings, Polimery 60 No. 4 (2015) 258-263.

[64] Sun, Z., Hu, X., Chen, H., Effects of aramid-fibre toughening on interfacial fracture toughness of epoxy adhesive joint between carbon-fibre face sheet and aluminium substrate, Int. J. of Adhesion & Adhesives 48 (2014) 288–294.